A novel hybrid system for the fabrication of a fibrous mesh with micro-inclusion

ARTICLE *in* CARBOHYDRATE POLYMERS · JUNE 2012

Impact Factor: 4.07 · DOI: 10.1016/j.carbpol.2012.02.074

Carbohydrate Polymers 89 (2012) 222–229

Contents lists available at SciVerse ScienceDirect

Carbohydrate Polymers

journal homepage: www.elsevier.com/locate/carbpol

A novel hybrid system for the fabrication of a fibrous mesh with micro-inclusions

Bilal Ahmad[a], Oguzhan Gunduz[a,b], Simeon Stoyanov[c], Eddie Pelan[c], Eleanor Stride[a,d], Mohan Edirisinghe[a,*]

[a] Department of Mechanical Engineering, University College London, Torrington Place, London WC1E 7JE, UK
[b] Materials Department, Technical Education Faculty, Marmara University, Goztepe, Istanbul 34722, Turkey
[c] Unilever Research, Olivier van Noortlaan 120, 3130 AC Vlaardingen, The Netherlands
[d] Institute of Biomedical Engineering, University of Oxford, Headington, Oxford OX3 7DQ, UK

ARTICLE INFO

Article history:
Received 3 February 2012
Received in revised form 27 February 2012
Accepted 29 February 2012
Available online 7 March 2012

Keywords:
Co-axial electrospinning
Microfluidics
Microbubbles
Particles
Fibrous mesh

ABSTRACT

A novel hybrid system combining microfluidic and co-axial electrospinning techniques has been used to generate different types of fibre structures with varied desirable inclusions using food grade polymers, ethyl cellulose and sodium alginate. The processing conditions in the microfluidic T-junction device, i.e. gas pressure and liquid flow rate were adjusted in order to generate near-monodisperse microbubbles which subsequently serve as a platform for particle generation. These particles exhibit micro-scale diameters and different shapes and some bubbles were incorporated into the fibrous mesh prepared by concurrent electrospinning. The fibre/particle structures obtained with different polymers via this novel method could potentially have many applications in various engineering and biological sectors.

1. Introduction

Control over structural parameters such as aspect ratio, in the case of fibre formation, and monodispersity, in the case of microbubbles, cannot be achieved via conventional methods such as drawing and sonication, respectively (Ramakrishna, Fujihara, Teo, Lim, & Ma, 2005; Unger et al., 2004). In contrast, electrospinning and microfluidic techniques offer better control over fibre and microbubble formation and have the added advantage of producing reproducible and, in the case of electrospinning, scalable structures (Dendukuri & Doyle, 2009; Seiffert, 2011; Seo et al., 2005; Stride, Pancholi, Edirisinghe, & Samarasinghe, 2008).

Since its inception over a century ago (Cooley, 1902; Morton, 1902), the primary focus of research into electrostatic fibre formation or "electrospinning" has been mostly the fundamental physics underlying the process (Doshi & Reneker, 1995; Feng, 2003) and its application in biomedical engineering for constructing wound dressings and tissue scaffolds for organ therapy (Agarwal, Wendorff, & Greiner, 2008). Electrospinning has emerged in recent years as a popular choice for producing continuous threads, fibre arrays and non-woven fabrics from a range of materials including polymers, ceramics, composites and food-grade materials with a range of diameters (1–100 μm) (Ramakrishna et al., 2005; Wongsasulak et al., 2010). Electrospun fibres at this scale have a number of desirable characteristics such as very large surface area to volume ratio, flexibility to incorporate surface functionalities, and superior mechanical properties (e.g. stiffness and tensile strength) (Huang, Zhang, Kotaiki, & Ramakrishna, 2003). The potential of electrospinning has also been demonstrated to attain conformity between size and output rates of fibres (Petras et al., 2007). Furthermore, electrospinning is relatively a robust and simple technique to produce nanofibres which offer several additional advantages such as adjustable porosity and the ability to produce structures with a wide vareity of sizes and shapes. Because of these advantages, electrospun nanofibres have also been widely investigated for its use in applications such as filtration, optical and chemical sensors and as electrode materials (Liang, Hsiao, & Chu, 2007). However, a well known limitation of the electrospinning process is the level of fibre productivity, which is very much lower than that of a current fibre technology (Teo & Ramakrishna, 2006). A simple method of increasing the productivity of electrospinning has been illustrated by the increase in the number of spinnerets used in the process (Ding, Kimura, Sato, Fujita, & Shiratori, 2004). While the production speeds of fibre formation have increased, other disadvantages to the electrospinning process that have been deterrents to the manufacturing on a large scale include safety and environmental issues of the toxic solvents used in the spin dopes and the high voltages involved in the electrospinning process. Moreover, solvent removal and recovery increase manufacturing costs. One of the ways forward is to develop polymer/solvent

* Corresponding author.
E-mail address: m.edirisinghe@ucl.ac.uk (M. Edirisinghe).

0144-8617/$ – see front matter © 2012 Elsevier Ltd. All rights reserved.
doi:10.1016/j.carbpol.2012.02.074

systems that are benign in terms of safety and environmental impact.

Recent studies have also investigated electrospun fibre membranes as being capable of molecular recognition (Hunley & Long, 2008). Incorporating functional molecules within electrospun fibres allows molecular imprinting of the polymer fibres (Hunley & Long, 2008). Electrospun fibres with inclusions can improve their functionality, however, their application has been limited so far due to molecule size and because molecules have to be added to the electrospinning solution prior to fibre formation (Hunley & Long, 2008). This facet of electrospinning could be extended further if bubbles or particles could be incorporated into the electrospun fibres via an *in situ* process. One such process is microfluidics, which has shown to generate generate homogeneous particles and monodisperse bubbles (Gunduz, Ahmad, Stride, Tamerler, & Edirisinghe, 2012; Whitesides, 2006). By combining both techniques it would be possible to include bubbles and particles into electrospun fibres. The application of such structures could potentially be immense as fibres and bubbles, consisting of various materials, would be created independently of each other and then combined to form one structure via an *in situ* process. In this work we have combined electrospinning and microfluidic techniques to produce fibres containing microbubbles/particles using food grade polymers; namely: ethyl cellulose and alginate.

2. Experimental setup

2.1. Materials

To create microbubbles and fibres, two solutions of sodium alginate (Alginic acid sodium salt, Sigma–Aldrich, Poole, UK) (solution 1) and ethyl cellulose ($M_w \sim 22{,}800$, Sigma–Aldrich, Poole, UK) (solution 2) were prepared. 25 mg of alginate was dissolved in 20 ml of deionised water and stirred in a plastic bottle with a magnetic stirrer for approximately 1 h and ethyl cellulose was dissolved in 10 ml of a binary solvent system of ethanol (BDH Laboratory Supplies) and water (80:20) at 25 wt.% of the polymer and stirred for 2 h.

2.2. Characterisation of solvents and solutions

The physical properties of the liquids: viscosity, surface tension and electrical conductivity were measured using a viscometer (Brookfield DV-III Ultra), Kruss tensiometer and a HANNA HI 8733 conductivity meter, respectively. Each device was calibrated using ethanol prior to the measurements.

2.3. FTIR spectroscopy

Fourier transform infrared (FT-IR) spectra of untreated powder ethyl cellulose, sodium alginate and ethyl cellulose-alginate were obtained using a PerkinElmer System 2000 FT-IR spectrometer (PerkinElmer Life and Analytical Sciences, Inc., Wellesley, MA, USA). Each sample powder was finely grounded with potassium bromide (KBr), a specially purified salt used to remove the scattering effects from large crystals (the mass ratio of the sample:KBr was 1:100). The powder mixture was then moulded in a mechanical die press to form a translucent pellet through which the beam of the spectrometer could pass.

2.4. Design and construction of novel device

A microfluidic T-junction device (dimensions: 22 mm × 22 mm × 15 mm) was constructed using poly(methylmethacrylate) (PMMA) by CNC machining, as shown in Fig. 1, and designed to withstand high gas pressures (>100 kPa) during the microbubbling process. High pressure Polytetrafluoroethylene (PTFE) polymer tubing (150 μm ID, Thames Restek, Saunderton, UK) was used for the capillaries infusing the alginate solution and nitrogen gas into the T-junction. The outlet capillary of the T-junction was connected to a co-axial stainless steel needle (outer-needle, ID ~ 810 μm, Stanley Engineering, Birmingham, UK)

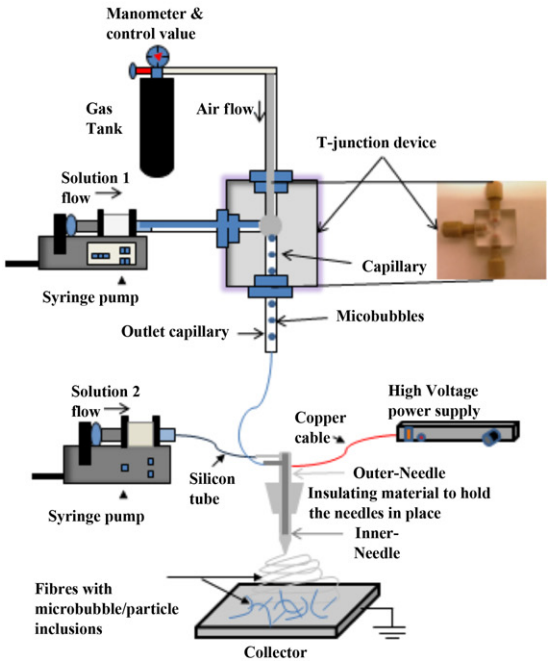

Shape	Fibre/particle/bubble size	Application
Short fibre/bubble mesh	Bubble Ø (20-150 μm) Fibre Ø (1-50 μm) (Fig. 2)	Biomedical engineering (Gomes et al., 2008), Biological application (Amitai et al., 2010)
Hollow and porous short fibres	Fibre Ø (1-10 μm) (Fig. 6)	Drug encapsulation and Food filteration (Srivastava et al., 2007;Tasselli et al., 2009). Biosensing (Swicka et al., 2005), Electronics (Babel et al., 2005), Food foams (Ahmad et al., 2011 and Tissue engineering (Pham et al., 2006)
Spherical and hollow particles in fibre matrix	Fibre Ø (1-30 μm) Particle Ø (1-50 μm) (Fig. 7)	Controlled drug delivery and pharmaceutical applications (Vehring, 2008), Therapeutic applications (Meier, 2000)

Fig. 1. A schematic diagram of the novel hybrid system combining the two techniques of microfluidics and electrospinning. The image clearly shows where the bubbles are formed and how the outlet capillary carries them to the co-axial electrospinning setup. The photograph is of the actual T-junction device used in this study. It also lists the particle/fibre shape and size generated through this method in this study along with potential applications of such structures. Ø indicates diameter.

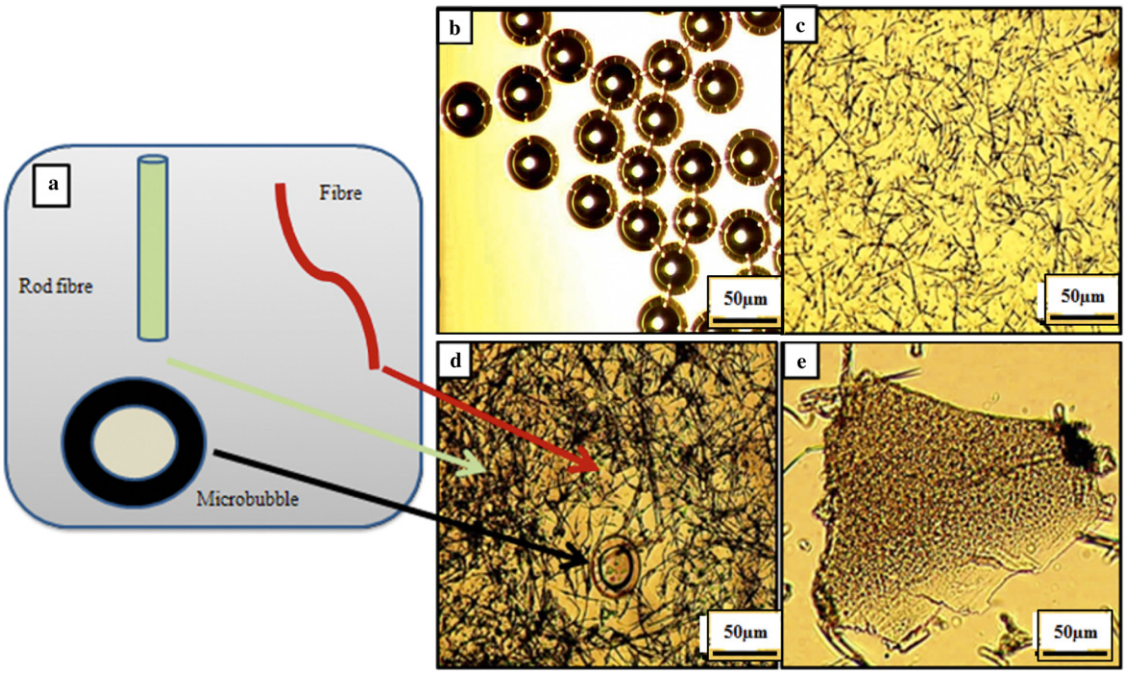

Fig. 2. (a) Schematic diagram of the structures produced in this investigation: microbubbles, rod-like fibres and fibres. Optical micrographs of (b) the near-monodispersed alginate microbubbles and (c) short ethyl cellulose fibres produced using this technique, and (d and e) particle/bubble structure in the fibrous mesh formed.

via a silicone tube (ID ~ 1 mm, VWR International Ltd, East Grinstead, UK). The inner needle (ID ~ 686 μm, Stanley Engineering, Birmingham, UK) was connected to the ethyl cellulose solution also via the silicone tube (ID ~ 1 mm, VWR, International Ltd, East Grinstead, UK).

2.5. Microfluidic bubble generation

At the junction, the capillaries were separated by a distance of 70 μm. The liquid flow rate was controlled using a 20 ml stainless steel syringe (KD Scientific, Holliston, MA, USA) mounted on a syringe pump (Harvard, PHD 4400). A valve with a manometer connected to the gas tank provided the required degree of control over the gas pressure. Initially, the air pressure was gradually increased until the pressure overcame the liquid's surface tension and a stream of bubbles was produced and collected from the outlet capillary at the bottom of the T-junction. The bubbles were immediately collected on glass slides and then observed under an optical microscope (Zeiss Axiotech) fitted with a Nikon Eclipse ME 600 camera to examine their size distribution.

2.6. Fibre electrospinning

Once stable microbubbling was achieved via the T-junction, ethyl cellulose solution was fed to the inner needle of the electrospinning arrangement. The liquid flow rate was controlled via a 10 ml plastic syringe mounted on a syringe pump (Harvard, PHD 4400). Voltage was applied to the liquid droplet exiting the outer needle of the co-axial needle setup via a high voltage power supply (FC 120 W, Glassman Europe Limited, Bramley, UK). The fibre/bubble structures formed via "microfluidic-co-axial electrospinning" were collected on dry and calcium chloride coated glass slides and observed under the optical microscope (Zeiss Axiotech) fitted with a Nikon Eclipse ME 600 camera before images were taken. The samples were then dried in air for 1 day, sputter coated with gold for 180 s and then analysed under the scanning electron microscope with an accelerating voltage of 5 kV.

3. Results and discussion

Amitai et al. (2010); Fig. 1 describes the types of structures produced via the novel hybrid system of "microfluidic co-axial electrospinning" and their possible applications. It has been shown through previous studies that each technique is capable of producing nano to micro scale structures provided that some pre-requisites are met in terms of materials and processing parameters. In the case of the microfluidic T-junction device, it has been reported that particles of a few micrometres in size were produced for applications in drug delivery and pharmaceutics (Gunduz et al., 2012). Similarly, it has been shown that nanofibres can be produced via the electrospinning technique on its own for applications in tissue engineering (Buttafoco et al., 2006). Combining the two techniques (hybrid system) could allow production of micro-scaled structures which contain both, micro particles and fibres. With more control over the processing parameters it may be possible to reach the nano-scale using this hybrid system. The detailed analysis of these structures and the technique used is discussed below.

3.1. Short fibre/bubble mesh

Fig. 2a illustrates the structures produced in this study: microbubbles, rod-like fibres and fibres from the alginate–ethyl cellulose solutions. In order to generate monodisperse microbubbles as seen in Fig. 2b, alginate solutions of various viscosities were tested. High viscosity alginate solutions ranging from 1000 to 1300 mPa s resulted in blockages within the T-junction system and too low viscosities ranging from 5 to 10 mPa s resulted in no microbubbles. The alginate solution eventually utilised (Table 1) was just viscous enough to form microbubbles but not cause any blockages in the T-junction. A liquid flow rate of 50 μl/min was first used to inject the alginate solution in to the T-junction. At the same time nitrogen gas was fed into the T-junction via the vertical capillary at low pressure. Once the optimal conditions were achieved (i.e. flow rate of 250 μl/min and gas pressure of

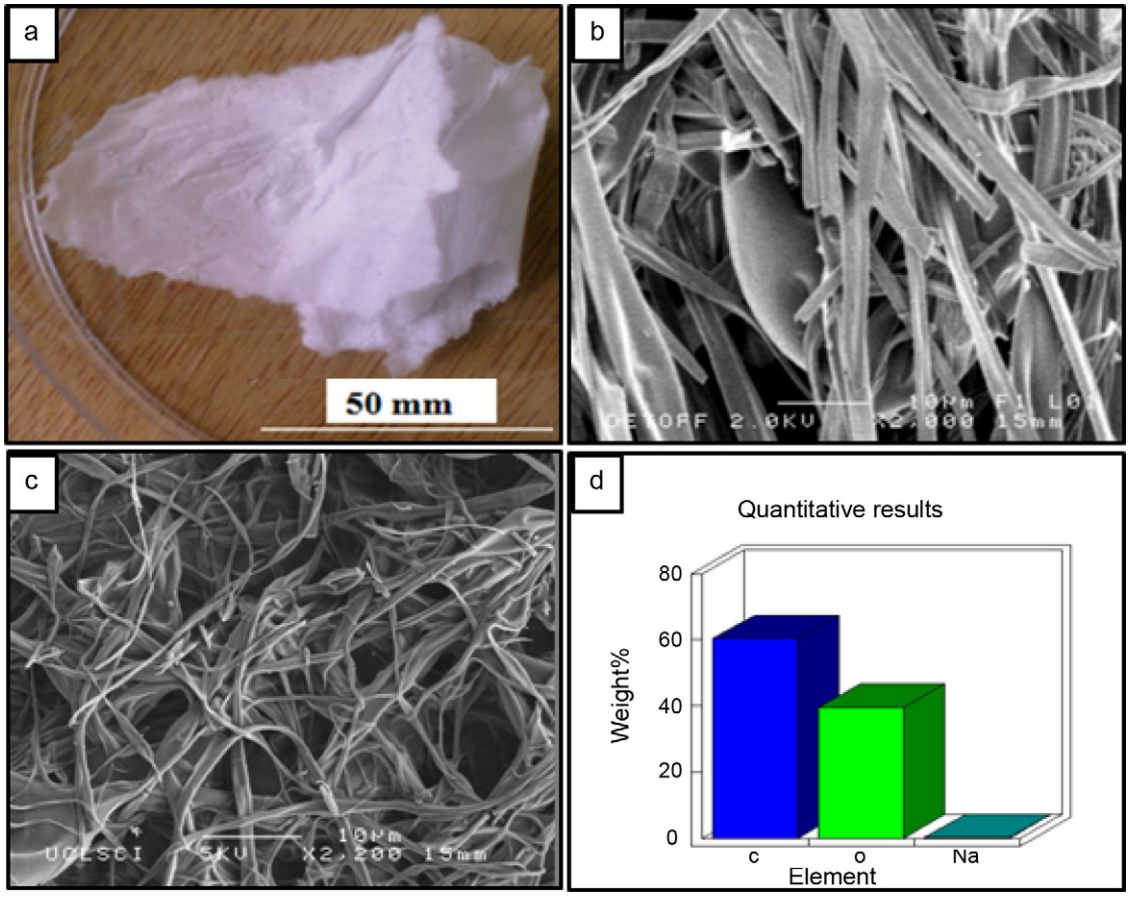

Fig. 3. (a) The alginate–ethyl cellulose fibrous structure, (b and c) scanning electron micrographs of the rod-like fibres and fibres, (d) element analysis of this structure showing carbon, oxygen and sodium.

100 kPa), near-monodisperse microbubbles were generated. The microbubble diameter was ~70 μm (Fig. 2b). The outlet capillary transported the microbubbles from the microfluidic T-junction to the co-axial needle setup via the inner needle, ready to be electrospun with ethyl cellulose fibres. High viscosity ethyl cellulose solution, 25 wt.% (Table 1) was injected into the outer needle of the co-axial needle setup at a flow rate of 50 μl/min. Once a droplet of ethyl cellulose exiting the outer needle was observed, voltage was applied to create an electric field between the needle tip and the grounded collector (Fig. 1). Initially, voltage was applied at small increments until a stable-cone jet was formed. The fibres started to emerge at 12 kV and reached optimum yield level at 14 kV. The fibre diameter ranged from 1 to 10 μm (Fig. 2c). The sample containing a mixture of alginate microbubbles and ethyl cellulose fibres were collected on to a glass slide and then on glass slides coated with calcium chloride (Fig. 2d and e). The addition of calcium chloride was to cross-link the alginate and to reinforce the structure. A fibrous mesh containing very small bubbles/particles started to form a few minutes in to the experiment (Fig. 3a). The accumulated mesh was easy to peel-off the grounded electrode and exhibited a tissue-like texture. The sample was stored for scanning electron microscopy (SEM) and element analysis to confirm the presence of alginate and ethyl cellulose.

Table 1
Properties of ethyl cellulose and alginate solutions used in this investigation. A dash indicates that accurate surface tension measurements with plate method were not possible due to the high viscosity of solution.

Solution	Viscosity (mPa s)	Surface tension (mN/m)	Electrical conductivity (S/m × 10^{-4})
Ethyl cellulose			
5%	23	25	47
10%	100	29	61
15%	363	36	68
20%	1230	54	84
25%	3692	–	80
30%	11,629	–	800
35%	14,600	–	1100
Alginate	13	63	67

The SEM images revealed a fibrous structure with short and rod-like fibres (Fig. 3b and c). The element analysis showed the presence of alginate and ethyl cellulose with strong peaks of carbon (C), oxygen (O) and trace amounts of sodium (Na) (Fig. 3d). FT-IR spectra were analysed to confirm the composition of the fibres and particles in the alginate–ethyl cellulose structure. Fig. 4 reveals infrared spectra of samples of pure ethyl cellulose powder, pure alginate powder and the alginate–ethyl cellulose sample over the wavenumber range from 400 to 4000 cm^{-1}. Some interaction, via the substituted hydroxyl groups among molecules of ethyl cellulose and the alginate–ethyl cellulose as well as hydroxyl groups, occurred (Fig. 4). Band A at 3479 cm^{-1} and band B at 3475 cm^{-1} were attributed to —OH stretching/vibration. In the alginate–ethyl cellulose sample, the shift from 3479 cm^{-1} to 3475 cm^{-1} and the fact that the peak also became wider is indicative of enhanced hydrogen bonding (Li & Yang, 2008). FTIR spectra of the Ca–alginate bond shown in Fig. 4a possess distinctive bands in the O—H region as stated before, and the carboxylic acid regions, 1380 and 1417 cm^{-1} which is consistent with the known structure of alginate polymer (Fig. 4c) (Stewart, Yau, Allen, Branbander, & Flyn, 2009).

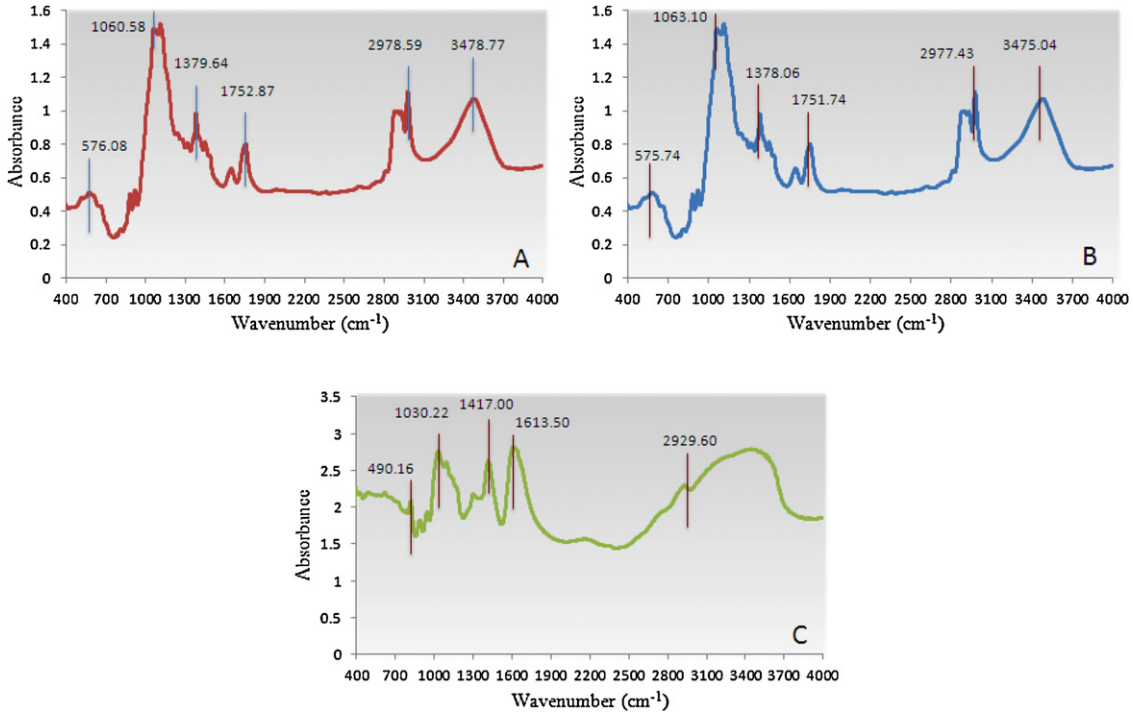

Fig. 4. (a) FT-IR spectra of alginate–ethyl cellulose samples, (b) pure ethyl cellulose and (c) pure alginate. Absorbance is in arbitrary units.

3.2. Hollow and porous short fibres with micro-inclusions

The key physical properties of the solutions which affect bubble generation and fibre formation in our method are viscosity (Stride et al., 2008; Wang et al., 2010) and surface tension, both of which are influenced by polymer concentration. Additional factors include gas type and pressure in the case of microfluidics which have been shown previously to affect microbubble generation (Ahmad, Stride, & Edirisinghe, in press; Stride et al., 2008). Increasing the gas pressure too much resulted in loss of near-monodisperse bubble generation (Fig. 5a). The morphology of the resulting fibres has been shown to be affected by many different variables in the electrospinning process. These include: solution composition and properties, applied voltage, collector type and distance from the collector and flow rate (Pham, Sharma, & Mikos, 2006). Low viscosity ethyl cellulose solutions (5–15 wt.%) (Table 1) resulted in electro spraying of droplets. No fibre formation occurred as the surface tension-electric field force compatibility was not conducive to electrospinning (Frey, 2008). The higher viscosity (30–35 wt.%) ethyl cellulose solutions resulted in thick droplets. Too high concentration (>35 wt.%) of ethyl cellulose solution resulted in needle blockages and therefore was not used for electrospinning. Another interesting trend observed during this study was the increase in surface tension and electrical conductivity with increasing viscosity of ethyl cellulose solutions (Table 1). Higher conductivity solutions are more favourable for jet formation and fibre spinning when subjected to high applied voltage (>12 kV) (Reneker & Chun, 1996). The particle–fibre–particle morphology (Fig. 5b) was also observed with our new method indicating the possibility for creating structures for applications in drug delivery. The encapsulation of drugs in particles has been shown before (Enayati, Ahmad, Stride, & Edirisinghe, 2010). The diameter of the fibre decreased (Fig. 5c and d) as its length increased due to electric forces accelerating and stretching the higher viscosity ethyl cellulose solutions (Pham et al., 2006). The fibres would reinforce this mesh by improving the overall mechanical properties of the structure. However, mechanical testing would be needed on the structures to confirm this hypothesis.

The gas and bubbles delivered from the T-junction into the coaxial needle also have an effect on the fibre morphology, with regions of deflated bubbles (Fig. 6a). Hollow and porous fibres are another type of structures produced with our technique (Fig. 6b and c) as the change in fibre diameter with high gas pressure results in fibre thinning with some fibres able to have diameters less than 2 μm (Fig. 6d) (Zhmayev, Cho, & Joo, 2010). With our method, fibre of different morphologies such as solid, hollow or porous at a micro-scale were made. The flow rate of alginate solution infused in to the T-junction was kept constant at 250 μl/min while the gas pressure was changed to 200 kPa, 320 kPa and 410 kPa to obtain solid, hollow and porous fibres, respectively. All the other processing parameters such as ethyl cellulose flow rate (50 μl/min) and concentration (25 wt.%), applied voltage (14 kV), collection distance from the nozzle tip (100 mm), collector type (glass slide coated with and without calcium chloride) were kept the same. The application of hollow and porous fibres and structures is extensive and includes, food filtration membranes and foams, biosensors, tissue engineered scaffolds, electronics and drug encapsulation (Ahmad et al., in press; Babel, Li, Xia, & Jenekhe, 2005; Pham et al., 2006; Srivastava et al., 2007; Swicka, Gouma, & Simon, 2005; Tasselli, Conidi, & Drioli, 2009). Our technique also allows the production of hollow and porous fibres with food grade solvents, with diameters <10 μm (Fig. 6b and c) compared with other similar studies (Frey, 2008).

3.3. Spherical and hollow particles

Particle formation was also observed in this study with fibres surrounding it. Many particles were obtained with fibres in the alginate–ethyl cellulose sample, some of which were non-spherical and possessed diameters less than 1 μm (Fig. 7a). Moreover, the particles seemed deflated when subjected to vacuum during SEM analysis as a result of being hollow. Hollow core spherical particles

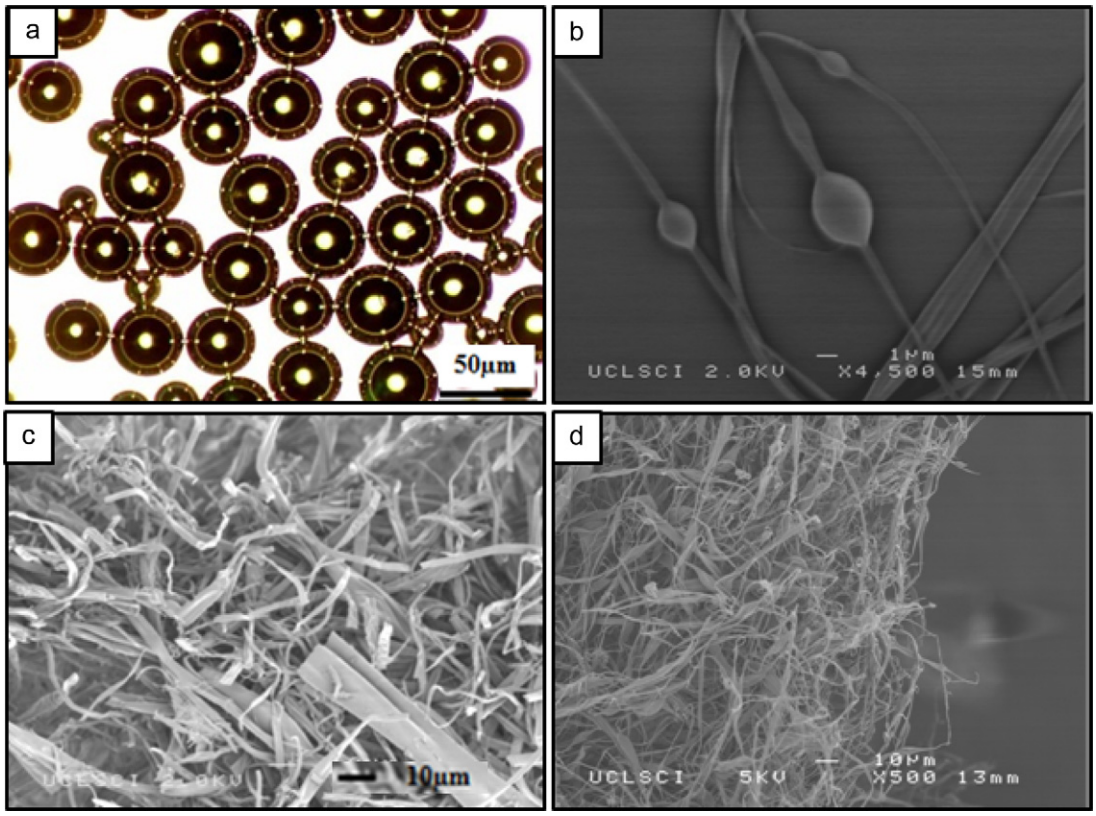

Fig. 5. (a) Optical micrograph of the polydisperse alginate microbubbles generated via the T-junction device. Scanning electron micrographs of (b) particle–fibre–particle morphology, (c) the fibrous mesh containing rod fibres and (d) cross-section view of the sample shown in Fig. 3a.

were also generated through the technique. The scanning electron micrographs indicate near spherical particles (Fig. 7b) with diameters just over 10 μm and in some instances these particles were connected to each other via a fibre (Fig. 7c). It is also evident through the SEM images that this technique also has the ability to produce particles which are hollow (Fig. 7d). The occurrence of such particles is highly dependent on gas pressure and type and the polymer solution to make the monodisperse microbubbles via the microfluidic T-junction device. With more control over bubble generation via the T-junction, these diameters can further be

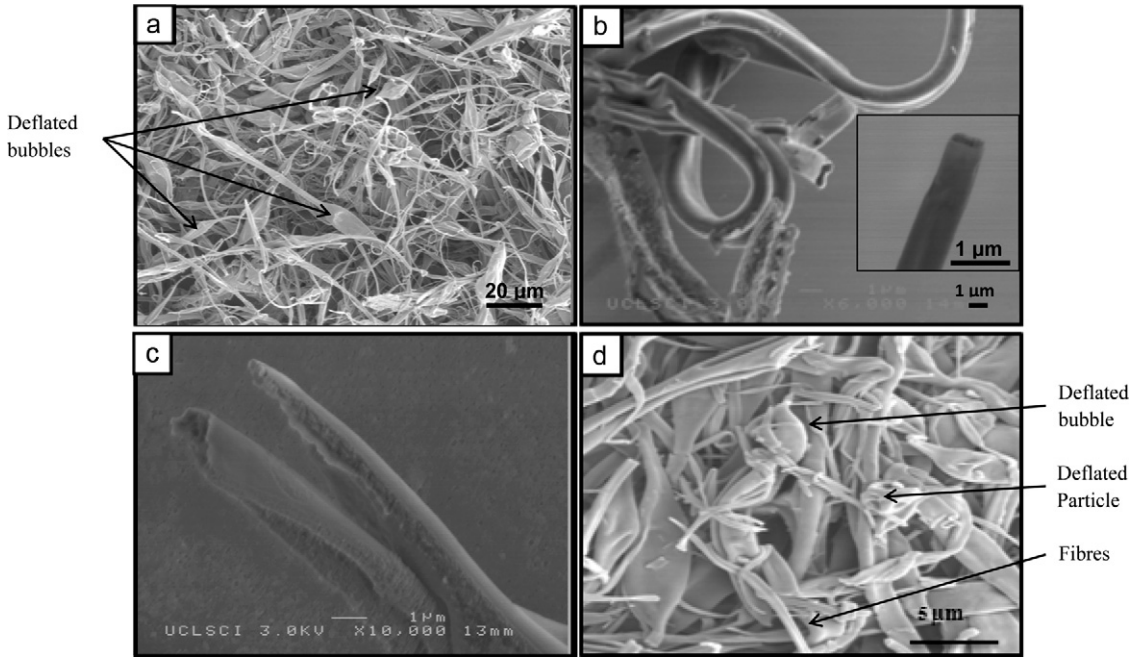

Fig. 6. Scanning electron micrographs of (a) deflated bubbles with fibres, (b) hollow fibres and a high magnification (×7500) image of a hollow fibre on the right side of the image, (c) porous fibres and (d) deflated particle, bubbles and fibres.

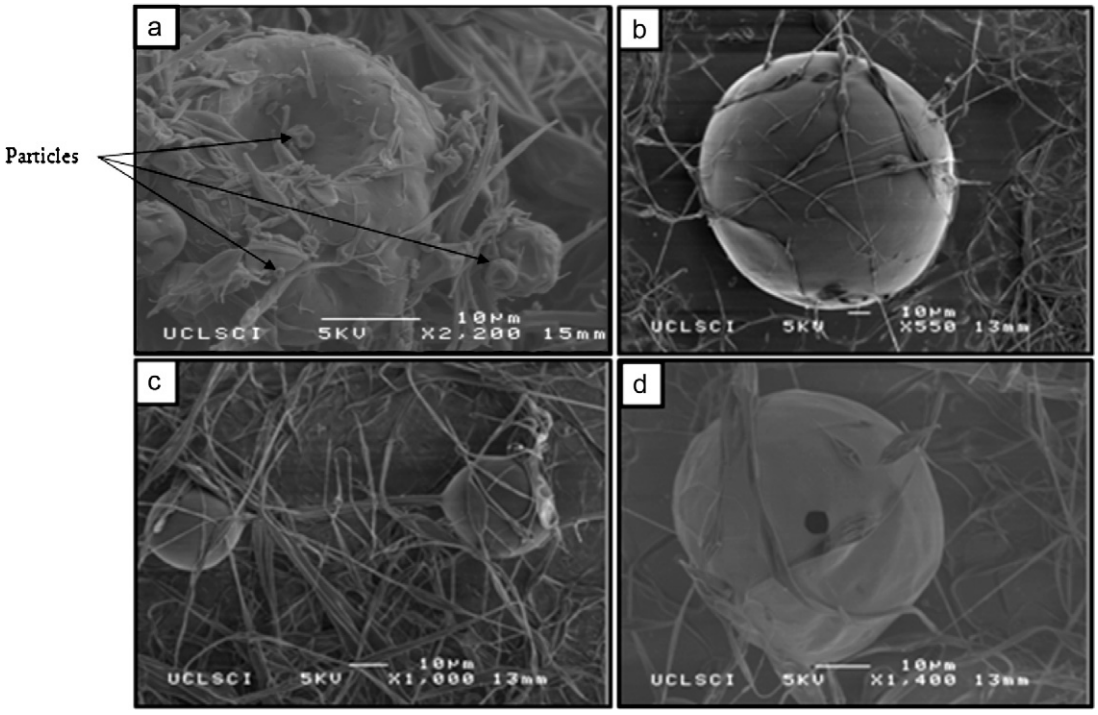

Fig. 7. Scanning electron micrographs of (a) low resolution image of many particles inside the fibre mesh, (b) near-monodisperse solid-core particle surrounded by fibres (1–50 μm diameter), (c) two spherical particles connected to each other via a fibre and (d) hollow particle in the fibre mesh.

reduced (Gunduz et al., 2012). The application of solid and hollow particles could potentially be immense in biotechnology such as controlled drug delivery and as therapeutic agents (Gunduz et al., 2012; Meier, 2000; Vehring, 2008). Combining the techniques in this way could also lead to the production of biocomposites containing fibres and microbubbles which have been used in the food industry as biofibre-soy based composites (John & Thomas, 2008). We have studied alginate and ethyl cellulose as a food grade polymer model to demonstrate the capability of this novel system of "microfluidic-co-axial electrospinning" to generate structures with the intention to use this technique with other biocompatible polymers.

4. Conclusions

In this work, we have developed a novel hybrid system to combine microfluidic and electrospinning techniques to generate near-monodisperse microbubbles/particles to be used as inclusions in fibres of various morphologies. Three types of particle and fibre structures were generated with this method, including a fibrous mesh containing deflated microbubbles, hollow and porous fibres and spherical hollow particles. The structures were reproducibly attained; experiments were repeated at least ten times to establish this. Particles and fibres had diameters ranging from 1 μm to 150 μm, and both structures acquired their structures independently to each other during the experimental stage with particles conforming to the size of microbubbles. The gas pressure and concentration of polymer solutions demonstrated a profound effect on the resulting structures size and uniformity. We used alginate and ethyl cellulose as an example to illustrate the concept behind this novel technique to generate structures useful in a whole host of applications and with the belief that same can be achieved with other biocompatible polymers. Future work on this method will be aimed at producing controlled structures to be used in food engineering.

Acknowledgements

The authors would like to thank Unilever, EPSRC (doctoral research program of Bilal Ahmad) and Islamic Development Bank (doctoral research program of Oguzhan Gundaz) for providing the funding for this work. The authors would also like to thank the Archaeology Department at UCL for the use of their scanning electron microscopes in this study.

References

Agarwal, S., Wendorff, J. H., & Greiner, A. (2008). Use of electrospinning technique for biomedical applications. *Polymer*, *49*, 5603–5621.
Ahmad, B., Stride, E., & Edirisinghe, M. J. (in press). Calcium alginate foams prepared by a microfluidic T-junction system: Stability and food applications. *Food and Bioprocess Technology*, doi:10.1007/s11947-011-0650-3.
Amitai, G., Andersen, J., Koepsel, R., & Russell, A. J. (2010). Decontamination of chemical and biological warfare agents with a single multifunctional material. *Biomaterials*, *15*, 4417–4425.
Babel, A., Li, D., Xia, Y. N., & Jenekhe, S. A. (2005). Electrospun nanofibres of blends of conjugated polymers: Morphology, optical properties, and field effect transistors. *Macromolecules*, *38*, 4705–4771.
Buttafoco, L., Kolkman, N. G., Engbers-Buijtenhuijs, P., Poot, A. A., Dijkstra, P. J., Vermes, I., et al. (2006). Electrospinning of collagen and elastin for tissue engineering applications. *Biomaterials*, *27*, 724–734.
Cooley, J. F. (1902). *Apparatus for electrically dispersing fluids*. US patent 692631.
Dendukuri, D., & Doyle, P. S. (2009). The Synthesis and assembly of polymeric microparticles using microfluidics. *Advanced Materials*, *21*, 1–16.
Ding, B., Kimura, E., Sato, T., Fujita, S., & Shiratori, S. (2004). Fabrication of blend biodegradable nanofibrous nonwoven mats via multi-jet electrospinning. *Polymer*, *45*, 1895.
Doshi, J., & Reneker, D. H. (1995). Electrospinning and applications of electrospun fibers. *Journal of Electrostatics*, *35*, 151–160.
Enayati, M., Ahmad, Z., Stride, E., & Edirisinghe, M. J. (2010). One-step electrohydrodynamic production of drug-loaded micro and nanoparticles. *Journal of The Royal Society Interface*, *7*, 667–675.
Feng, J. J. (2003). Strecthing of a straight electrically charged viscoelastic jet. *Journal of Non-Newtonian Fluid Mechanics*, *116*, 55–70.
Frey, M. W. (2008). Electrospinning cellulose and cellulose derivatives. *Polymer Reviews*, *48*, 378–391.
Gomes, M. E., Azevedo, H. S., Moreira, A. R., Ella, V., Kellomaki, M., Reis, R. L., et al. (2008). Starch–poly(ε-caprolactone) and starch–poly(lactic acid) fibre-mesh scaffolds for bone tissue engineering applications: Structure, mechanical

properties and degradation behaviour. *Journal of Tissue Engineering and Regenerative Medicine*, *2*, 243–252.
Gunduz, O., Ahmad, Z., Stride, E., Tamerler, C., & Edirisinghe, M. (2012). Bioinspired bubble design for particle generation. *Journal of Royal Soiety Interface*, *9*(67), 389–395.
Huang, Z. M., Zhang, Y. Z., Kotaiki, M., & Ramakrishna, S. (2003). A review on polymer nanofibers by electrospinning and their applications in nanocomposites. *Composites Science and Technology*, *63*, 2223.
Hunley, M. T., & Long, T. E. (2008). Perspective Electrospinning functional nanoscale fibres: A perspective for the future. *Polymer International*, *57*, 385–389.
John, M. J., & Thomas, S. (2008). Biofibres and biocomposites. *Carbohydrate Polymers*, *71*, 343–364.
Li, X. W., & Yang, T. F. (2008). Fabrication of ethyl cellulose microspheres: Chitosan solution as a stabilizer. *Korean Journal of Chemical Engineering*, *25*, 1201–1204.
Liang, D., Hsiao, B. S., & Chu, B. (2007). Functional electrospun nanofibrous scaffolds for biomedical applications. *Advanced Drug delivery Reviews*, *59*, 1392–1412.
Meier, W. (2000). Polymer nanocapsules. *Chemical Society Reviews*, *29*, 295.
Morton, W. J. (1902). *Method of dispersing fluids*. US patent 705691.
Petras, D., Mares, L., Cmelik, J., & Fiala, K. (2007). *Device for production of nanofibres by electrostatic spinning of polymer solutions*. Patent WO/2007/137530.
Pham, Q. P., Sharma, U., & Mikos, A. G. (2006). Electrospinning of polymeric nanofibers for tissue engineering applications: A review. *Tissue Engineering*, *12*, 1197–1211.
Ramakrishna, S., Fujihara, K., Teo, W. E., Lim, T. C., & Ma, Z. (2005). *An introduction to electrospinning and nanofibers*. Singapore: World Scientific. Chapter 1
Reneker, D. H., & Chun, I. (1996). Nanometre diameter fibres of polymer produced by electrospinning. *Nanotechnology*, *7*, 216.
Seo, M., Nie, Z. H., Xu, S. Q., Lewis, P. C., Graham, R., Mok, M., et al. (2005). Continuous microfluidic reactors for polymer particles. *Langmuir*, *21*, 11614.
Seiffert, S. (2011). Functional microgels tailored by droplet-based microfluidics. *Macromolecular Rapid Communications*, *32*, 1600–1609.
Srivastava, Y., Loscertales, I., Marquez, M., & Thorsen, T. (2007). Electrospinning of hollow and core/sheath nanofibres using a microfludic manifold. *Microfluidics and Nanofluidics*, *4*, 245–250.
Stewart, T. J., Yau, J-H., Allen, M. M., Branbander, D. J., & Flyn, N. T. (2009). Impacts of calcium-alginate density on equilibrium and kinetics of lead (II) sorption onto hydrolgel beads. *Colloid Polymer Science*, *287*, 1033–1040.
Stride, E., Pancholi, K., Edirisinghe, M. J., & Samarasinghe, S. (2008). Increasing the nonlinear character of microbubble oscillations at low acoustic pressures. *Journal of The Royal Society Interface*, *5*, 807.
Swicka, K., Gouma, P., & Simon, S. (2005). Electrospun biocomposite nanofibres for urea biosensing. *Sensors and Actuators B: Chemical*, *108*, 585–588.
Tasselli, C. F., Conidi, C., & Drioli, E. (2009). Ultrafiltration of clementine mandarin juice by hollow fibre membranes. *Desalination*, *241*, 302–308.
Teo, W. E., & Ramakrishna, S. (2006). A review on electrospinning design and nanofibre assemblies. *Nanotechnology*, *17*, R89–R106.
Unger, E. C., Porter, T., Culp, W., Labell, R., Matsunaga, T., & Zutshi, R. (2004). *Advanced Drug Delivery Review*, *56*, 1291–1314.
Vehring, R. (2008). Pharmaceutical particle engineering via spray drying. *Pharmaceutical Research*, *25*, 5.
Wang, X., Li, X., Stride, E., Huang, J., Edirisinghe, M., Schroeder, C., et al. (2010). Novel preparation and characterisation of porous alginate films. *Carbohydrate Polymers*, *79*, 989–997.
Whitesides, G. (2006). The origins and the future of microfluidics. *Nature*, *442*, 368–373.
Wongsasulak, S., Patapeejumruswong, M., Weiss, J., Supaphol, P., & Yoovidhya, T. (2010). Electrospinning of food-grade nanofibres from cellulose acetate and egg albumen blends. *Journal of Food Engineering*, *98*, 370–376.
Zhmayev, E., Cho, D., & Joo, Y. K. (2010). Nanofibres from gas assisted polymer melt electrospinning. *Polymer*, *51*, 4140–4144.